Dissolution-DNP enables the detection of ^{13}C hyperpolarized NMR spectra of Li-ion battery electrolytes

Chloé Gioiosa[†1,2], Ekaterina V. Pokochueva[1], James Tolchard[1], Charlotte Bocquelet[1], Mohamed Ayman Ennachet[1], Nghia Le[1,3], Laurent Veyre[3], Anne Lesage[1], Ségolène Laage[2], Simon Pondaven[2], and Sami Jannin[1]

[1] *Université Claude Bernard Lyon 1, CRMN UMR-5082, CNRS, ENS Lyon, Villeurbanne 69100 France*

[2] *TotalEnergies OneTech, Centre de recherche de Solaize, Chemin du Canal, 69630 Solaize, France*

[3] *Université de Lyon, Institut de Chimie de Lyon, Laboratory of Catalysis, Polymerization, Processes and Materials, CP2M UMR 5128 CNRS-UCB Lyon 1-CPE Lyon, CPE Lyon 43 Bd du 11 Novembre 1918, 69616 Villeurbanne, France.*

[†] chloe.gioiosa@univ-lyon1.fr

Abstract: Dissolution Dynamic Nuclear Polarization (dDNP) is a powerful hyperpolarization technique enabling sensitivity gains beyond four orders of magnitude in solution nuclear magnetic resonance (NMR). Over the last decades, researchers' efforts have led to an extension of dDNP applications in fields such as imaging, metabolomics, and drug discovery.

Lithium-ion batteries are one of the most widespread types of rechargeable batteries, which calls for a deeper understanding of the various physicochemical mechanisms involved in making them more efficient, safe, and sustainable. One of the key challenges lies in better understanding and limiting the degradation of the battery electrolyte, which can significantly impact the battery's performance. While NMR has been used in attempts to understand these mechanisms, notably by investigating the degradation products, the intrinsic lack of sensitivity of this technique, combined with the limited accessible volume of such compounds, makes its application often challenging.

In this work, we combine several state-of-the-art dDNP methodologies to acquire with high sensitivity solution ^{13}C NMR spectra of battery electrolytes. We show that we can successfully detect hyperpolarized ^{13}C signals on formulated battery electrolyte solutions on a 600 MHz spectrometer with sensitivity gains of up to 3 orders of magnitude. This work paves the way for studying lithium-ion battery electrolyte degradation under real usage conditions (cycling, thermal aging, air exposure…) with a ^{13}C detection limit below the micromolar range. This methodology has the potential to provide new insights into degradation mechanisms and the role and effectiveness of additives to mitigate electrolyte degradation.

Keywords: Batteries, Electrolytes, dDNP, Hyperpolarization, NMR, Li-ion.

Introduction

Dissolution Dynamic Nuclear Polarization (dDNP)[1] is a hyperpolarization technique used in magnetic resonance spectroscopy, enabling tremendous sensitivity enhancements, of more than four orders of magnitude. It involves doping a liquid sample with radical species, freezing the mixture in a DNP polarizer at very low temperatures (typ. 1.1-1.5 K), and subjecting electron spins' transitions to microwave irradiation, which ultimately leads to the hyperpolarization of the nuclear spins through various DNP mechanisms[2]. The frozen, hyperpolarized sample is then rapidly dissolved with hot pressurized solvent and transferred as a liquid to another nuclear magnetic resonance (NMR) spectrometer, where the hyperpolarized signal is recorded, allowing the acquisition of spectra within minutes that would have otherwise taken years to acquire at thermal equilibrium conditions. Since its discovery in 2003[1], dDNP has helped push the boundaries of magnetic resonance in several domains and has found many applications in magnetic resonance imaging[3–5], particularly in cancer detection[6–8], as well as in metabolomic studies[9,10], in biochemistry including protein studies[11], and drug discovery[12–14]. dDNP has now become an appealing alternative for research and innovation projects requiring the detection and characterization of low-concentrated species in limited sample volumes. One research subject that falls into that category is battery electrolytes, more specifically in lithium-ion battery technology[15].

Lithium-ion batteries (LiBS) have become highly popular, especially in small portable electronic devices, due to their high energy density, long lifespan, lightweight, and low self-discharge. However, with the increasing demand in areas such as electric vehicles and electric grid storage, existing solutions must be adapted and upgraded to meet new requirements in terms of capacity, fast charge, material sourcing, and overall lifetime. As a result, many studies and developments are carried out to make LiBS more performant, safer, and environmentally friendly. To achieve this, research teams have invested significant effort into better understanding the chemistry behind these batteries[16]. This includes studying the chemical reactions occurring during charge and discharge cycles[17], as well as identifying potential degradation products that could compromise the battery's lifetime, safety, and integrity[18]. Analyzing the electrolyte solution responsible for the ion transport in the battery is one way to gain insights into these mechanisms[19]. Several studies have already shown the central role of electrolytes in a battery as they are involved in degradation pathways[20] or Solid Electrolyte Interphase (SEI) formation[21], which eventually impacts the battery's overall performances[22]. Electrolyte solutions are therefore often reformulated and optimized by incorporating additives intended to prevent degradation and improve the battery's safety and performance[23,24]. Understanding the exact role of these additives, present in small quantities in the formulation, is another key stake in

battery development. One of the most effective analytical tools to address these questions is NMR[25] as it provides direct atomic-scale elucidation of molecular structures with high specificity as well as quantitative information. NMR has been extensively used to study LiBS electrolytes[26], providing means to better understand degradation pathways and interactions between the solvent and lithium salt [27,28], to probe additives' roles and impact on battery performances[29], and to yield insight into SEI formation[26]. Yet, many mechanisms in batteries remain far from being fully understood. Although NMR has proven itself a handy tool, its intrinsic lack of sensitivity strongly limits the study of low-concentrated species. Besides, NMR analysis is often limited by the low quantity of available sample volume. This is particularly true for battery electrolytes after cycling, for which only a small and variable amount of electrolyte, in the order of hundreds of microliters, is usually retrieved from a single pouch cell. The use of DNP is, therefore, an attractive prospect to get insights into the batteries' functioning through the study of their electrolyte solutions, as it could make the detection of low amounts of degradation products and additives possible on small sample volumes. However, applying the existing dDNP methodologies to study such samples is far from straightforward.

dDNP was initially developed to enhance sensitivity for metabolic imaging[30]. Therefore, most of its developments were tailored to study single molecules or simple mixtures soluble in water. With that in mind, classical dDNP sample formulations[31] usually involve a molecule solubilized in a mixture of deuterated solvents, including water, in proportions calculated to optimize the proton concentration of the overall sample for efficient DNP transfers. Stable radicals like trityl or nitroxides such as TEMPO are added to this mixture, together with a glassing agent such as glycerol. The latter promotes the formation of a glass upon freezing, leading to a homogeneous distribution of radicals. All these sample preparation prerequisites imply that the analyte must be relatively inert, insensitive to moisture or oxygen, and in a chemical environment that does not jeopardize the radical stability. Li-ion battery electrolytes do not fulfill the above requirements due to their high reactivity and sensitivity to air and moisture. When exposed to air, one degradation product formed is hydrofluoric acid (HF), which is known to be highly reactive. Furthermore, the conventional dDNP workflow usually involves exposing the sample to air during preparation, insertion into the polarizer spectrometer, and transfer to the NMR spectrometer[32]. Thus, using dDNP to study battery electrolytes requires new methodologies and instrumentation, and an adapted sample formulation to analyze the electrolytes without compromising their content.

Intense research and developments on pulse sequences, hardware, and sample formulation have transformed dDNP into a more versatile, universal technique. In particular, the introduction of multiple cross-polarization (CP) steps[33–35] together with microwave gating[36] has enabled the hyperpolarization of low-gamma nuclear spins at natural abundance in complex mixtures in a faster, more efficient manner[9,10]. Implementing fast transfer and injection systems, including helium back pressure[37,38] and magnetic tunnels[39], enabled the transfer and injection of the sample with limited exposure to air, and the observation of molecules with increasingly shorter longitudinal relaxation time, expanding the pool of molecules that can be studied through dDNP.

Samples and their formulation have also become more diverse: dDNP now allows for the analysis of complex mixtures for metabolomics[9,10], and some more exotic sample formulations involving hydrophobic solvents have also been reported[40,41], notably to monitor polymerization intermediates. These recent improvements, if properly used together, open the way to dDNP analysis of reactive and air- or water-sensitive samples, such as battery electrolytes.

In this paper, we propose to combine these state-of-the-art dDNP methodologies[32] with innovative sample preparation protocols to make dDNP analysis of battery electrolytes possible. The sample formulation was adjusted by eliminating the use of the deuterated solvents and glassing agents, and directly adding TEMPO radicals into the electrolyte solutions. DNP was performed using ^{13}C multiple cross-polarization (multi-CP) steps along with microwave gating. The dissolution conditions were also revisited by replacing water as a dissolution solvent with isopropanol which showed perfect compatibility with our fast transfer system. The hyperpolarized ^{13}C NMR spectrum of a commercial electrolyte solution could then be acquired. We demonstrate that this method enables the detection of natural abundance hyperpolarized ^{13}C signals on formulated battery electrolyte solutions. Signal enhancements ranging from 350 to 3300 on different carbon types could be obtained, leading to sub-millimolar detection limits on a single scan acquisition. Moreover, we also show that the method proves itself useful for probing degradation products in degraded electrolyte formulas. We believe this methodology will offer a fresh perspective on dDNP applications, particularly in the field of battery research, and will pave the way for further investigations of these types of samples.

Results and discussion

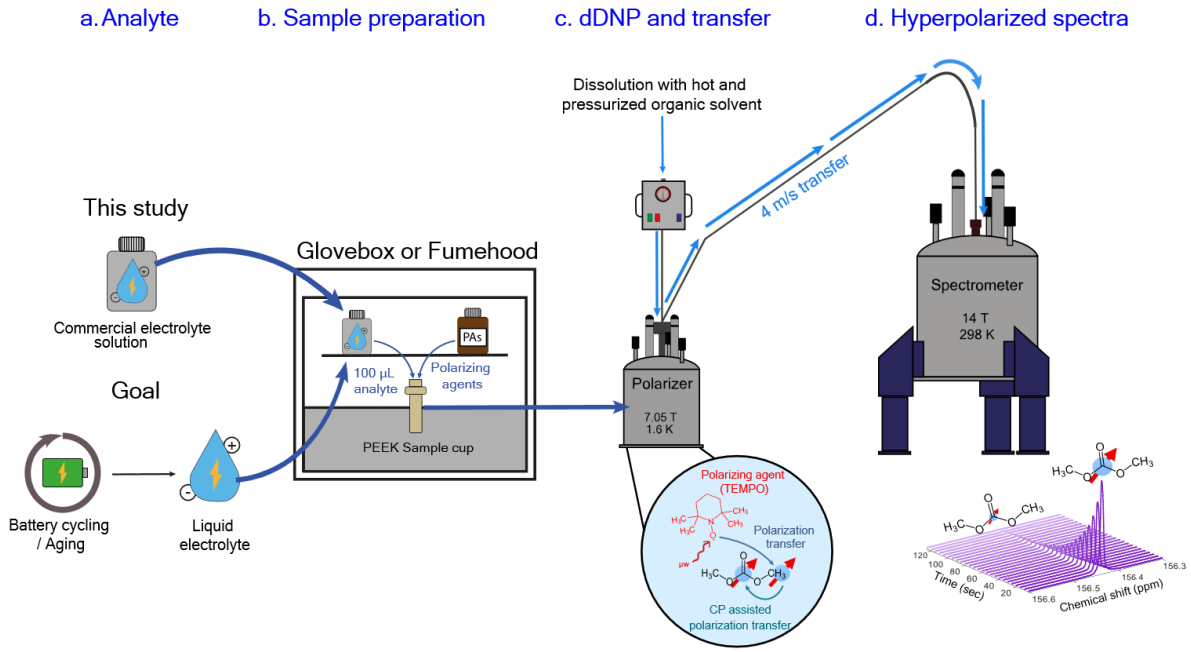

Figure 1: Illustrative scheme of the methodology and setup used to perform dDNP on battery electrolytes. a. Commercial electrolyte solutions b. are mixed with polarizing agents. c. The mixture is then inserted in a dDNP polarizer operating at 7.05 T and 1.6 K. The sample is irradiated with microwaves for DNP and radio-frequency pulses for CP. The sample is then dissolved and melted with an adequate organic solvent, d. and is injected directly in the liquid state to a 14 T NMR spectrometer to perform the acquisition of the hyperpolarized signal at room temperature.

Figure 1 illustrates the workflow and setup used for this study. A commercial "LP30" electrolyte solution composed of 1M lithium hexafluorophosphate ($LiPF_6$) salt solubilized in a mixture of ethylene carbonate (EC) and dimethyl carbonate (DMC) (50/50, v/v), was used to test the feasibility of the experiment, and ultimately to replicate the method on cycled/degraded electrolytes, directly withdrawn from a battery cell. Sample preparation was a key step as it had to balance DNP efficiency and sample integrity. It was found that the simplest strategy to prepare the solution for DNP was to add the hyperpolarizing agents directly to the electrolyte sample. The carbonate solvents act as self-glassing agents, preventing radicals from forming clusters in the sample once frozen. No deuterated solvents were used. The commonly used TEMPOL radical, mostly insoluble in such media, was simply replaced by its hydroxyl group-free version: TEMPO, which displayed better solubility in the electrolyte solution.

For this study, sample preparation was performed under a fume hood in less than 10 minutes. The potential electrolyte degradation caused by the brief air exposure was negligible, as confirmed later by control experiments (see Figure S1 in SI). However, if needed, this step could also be performed under an inert atmosphere inside a glovebox, to limit sample exposure to air.

This study focused on analyzing ^{13}C nuclear spin hyperpolarization. Observing carbonates-based electrolyte solvents with dDNP was considered a promising and relevant approach. The electrolyte solvent plays an important role in the battery as it participates in SEI formation, ensures efficient ion conductivity, and is involved in degradation pathways[19,42,43]. In addition, carbonate species carry a carbonyl group, which usually displays a long longitudinal relaxation time T_1 in solution, ensuring a slow polarization decay, making them suitable candidates for dDNP.

The remainder of the dDNP experiment followed a conventional experimental workflow used in the group[32]. Sample polarization is performed through electron-to-proton polarization transfer induced by irradiating the sample with microwaves. Proton polarization builds up and is transferred to ^{13}C through multi-CP experiments[33]. The usual D_2O dissolution solvent was replaced with deuterated isopropanol, which can be readily heated up to approximately 160°C while pressurizing it below the 15 bars threshold of our heating box system and displays satisfactory viscosity properties for the transfer. It also displays good affinity with the electrolyte while remaining safe for the fast injection system. The hyperpolarized ^{13}C solution NMR spectrum could then be acquired at 14 T with a single $\pi/2$ pulse to maximize the signal intensity.

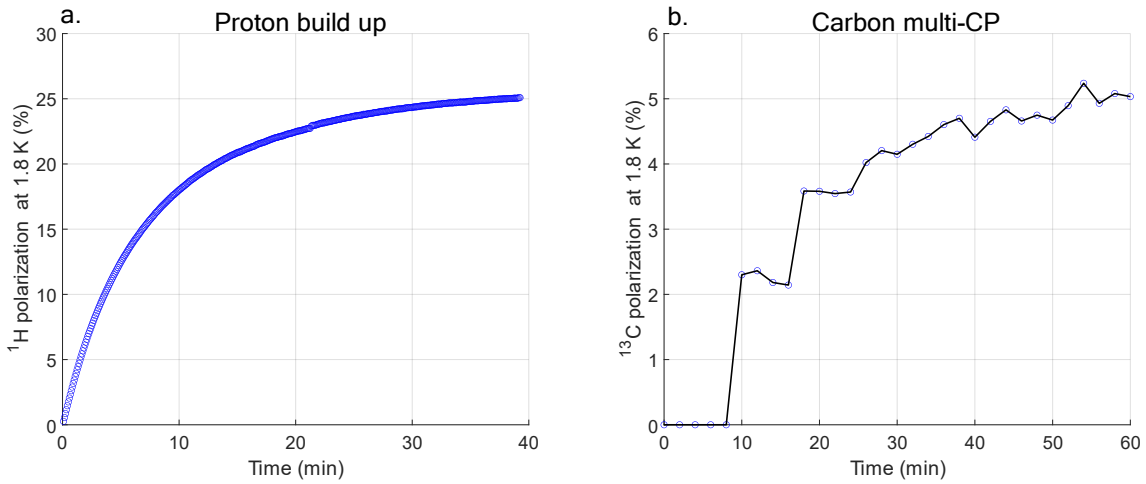

Figure 2: a. ^{1}H DNP polarization buildup and b. ^{13}C multi-CP induced polarization buildup of 100 µL commercial electrolyte (EC/DMC, 50/50, v/v, +1M $LiPF_6$) doped with 50 mM TEMPO measured at 7.05 T and 1.8 K with microwave irradiation frequency $f_{\mu w}$ = 197.7 GHz. Blue dots on the proton build-up correspond to the polarization values calculated from the integrals of each experimental data point over time, recorded every 5 seconds with 64 scans and small flip angles of 0.1°. The data points were then fitted with a stretched mono-exponential function to extract the build-up time. Blue dots on the carbon multi-CP correspond to the polarization values calculated from the integrals of each experimental data point over time, recorded every 180 seconds with 1scan and small flip angles of 5°. The solid black line only serves as a visual guide.

Figure 2 shows the ^{1}H polarization build-up and ^{13}C multi-CP-assisted ^{13}C polarization build-up of the commercial electrolyte sample at 1.8 K. Under these conditions, the maximum ^{1}H polarization attained was estimated to be P_{1H} = 25% after 40 minutes of experiment. An hour-long multi-CP-assisted ^{13}C polarization build-up experiment was then carried out. The final ^{13}C polarization was estimated to be around P_{13C} = 5~10%. The low signal-to-noise ratio, caused by the 1.1% natural abundance of ^{13}C, combined with the small 5° pulses used to preserve polarization during signal monitoring, makes it difficult to quantify the solid-state ^{13}C signal with high accuracy.

The ^{13}C polarization levels are lower than what is usually achieved for more conventional dDNP sample formulations, typically reaching up to P_{13C} = 65% (see Table S1 in SI). Indeed, sample preparation was not tailored here to ensure optimum DNP, for example, by diluting with a deuterated solvent. Sample formulation was kept identical to the native electrolyte solution, and it is demonstrated that DNP can be performed after a simple addition of the radicals. These results demonstrate that DNP can work with minimal and fast sample preparation which has the power to significantly increase detection sensitivity in complex samples such as battery electrolytes.

The build-up time for ^{1}H polarization was found to be longer compared to a more optimized sample formulation. A τ_{DNP} of 8 min was observed for this formulation instead of 4 min for a fully optimized electrolyte sample formulation involving significant dilution in deuterated toluene (see Figure S2 in SI). For sensitivity and sample preservation during the DNP process, a 2-times longer build-up time is preferred to a >10-fold sample dilution.

These lower polarization values and longer build-up times could be explained by a combination of i) a high proton concentration (three times more compared to optimal proton concentrations usually used under these dDNP conditions), and ii) a lower radical concentration likely due to a partial quenching by the electrolyte during the sample transfer and insertion in the polarizer, right before freezing.

Figure 3 shows the ^{13}C proton-decoupled spectrum of the commercial electrolyte solution after being hyperpolarized and dissolved, and the spectrum of the same solution recorded after relaxation to thermal equilibrium. On the spectrum of hyperpolarized electrolyte, all carbonate peaks could be detected and identified with signal-to-noise ratios (SNR) exceeding 1000 and a resolution better than 10 ppb. Such resolution enabled to readily resolve both carbonate carbonyl signals despite very close chemical shifts (156.5 ppm for ethylene carbonate, and 156.4 ppm for dimethyl carbonate).

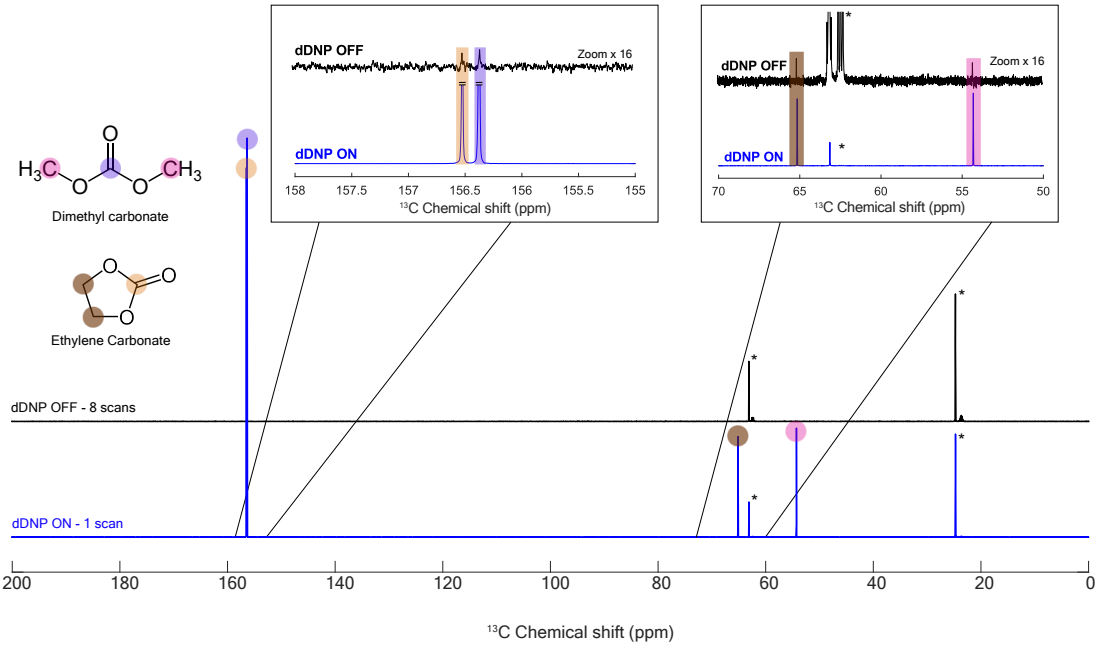

Figure 3 : Comparison of proton decoupled ^{13}C hyperpolarized spectrum of a 100 µL commercial electrolyte (EC and DMC 50/50, v/v + 1M $LiPF_6$) mixed with 50 mM TEMPO, hyperpolarized through dDNP at 1.8 K in a 7.05 T Bruker Polarizer through multi-CP experiment, rapidly dissolved with 7 mL of an isopropanol mixture (isopropanol/isopropanol-d_8, 3/1, v/v) and detected in a 14 T spectrometer equipped with a cryoprobe with a 90° detection pulse (blue). The thermal equilibrium proton decoupled ^{13}C spectrum of the same sample, in the same spectrometer, was recorded with 8 scans, after completing dissolution and relaxation of the nuclear spins (black). The 155 to 158 ppm region of the spectra where the signals of EC (yellow) and DMC (purple) carbonyl groups are observed was zoomed in, as well as the 50 to 70 ppm region for EC CH_2 (brown) and DMC CH_3 groups (pink). Signals marked with a star correspond to isopropanol signals.

Table 2 summarizes the dDNP experiment's performances for the two carbonate species in terms of enhancements, signal-to-noise ratios (SNR), and limits of detection (LOD). All carbons were assigned, and the comparison between signals from the hyperpolarized state and thermal equilibrium allowed us to determine the overall sensitivity gain.

Table 2: Summary table of the dDNP experiments results on commercial electrolyte solution (Figure 3) with identified carbon species for each molecule and their chemical shifts δ, calculated enhancements, signal-to-noise ratios (SNR) and estimated final limit of detection (LOD) for a given SNR of 5.

	Ethylene carbonate (EC)		*Dimethyl Carbonate (DMC)*	
Carbon type	C=O	CH_2	C=O	CH_3
δ (ppm)	156.5	65.2	156.4	54.35
Enhancement	3000	350	3300	450
SNR	4200	1140	4700	1200
Final estimated LOD	30 µM	100 µM	30 µM	100 µM

The ^{13}C enhancements span between 350 and 3300. Longitudinal relaxation times of carbonyl groups were measured to be around 30 seconds, while for CH_2 and CH_3 groups, these values were respectively 5 seconds and 6 seconds (see Figure S3 and Table S2 in SI). Such disparities in enhancements are rather unusual in our dDNP setting as our transfer time of 2 seconds (see methods) rarely exceeds nuclear spin-lattice relaxation times T_1. However, it can be explained here by the fact that we made the deliberate choice of adding a waiting time of 8 seconds before acquisition (see methods). Such waiting time provided an extended sample stabilization after injection and, therefore, a maximized NMR resolution.

The concentration after dissolution for each carbonate was estimated to be ca. 20 mM. The initial concentrations for EC and DMC were found to be 7.5 M and 5.4 M, respectively, corresponding to dissolution factors of 375 and 270. These values are much higher than the theoretical dissolution factor of 70 expected considering the 7 mL of solvent flushed on the 100 µL sample inside the polarizer. This is most likely due to an inhomogeneous concentration profile of the dissolved solution. Here, the selected part of the injected solution to the spectrometer wasn't optimized. This effect will be investigated in the future, to further improve the final SNR.

Given the enhancements and SNR observed on the hyperpolarized spectrum, the theoretical limits of detection were estimated at around 30 µM for C=O moieties and 100 µM for CH_2 / CH_3 moieties, for an SNR of 5. Consequently, all carbon groups could be detected with a single 90° scan for a concentration of natural abundance substrates after dissolution of 100 µM.

The largest enhancement was calculated to be 3300 for the C=O group of DMC. However, if we want to compare this enhancement to conventional NMR experiments, the amount of analyte should be considered. Typically, 100 µL of the sample is used for dDNP and diluted during dissolution (typically 50 to 300 times). For thermal equilibrium experiments, the dilution factor is generally 10. Therefore, the practical 'true' enhancement compared to conventional NMR is rather 100 to 600. Such enhancements might appear rather modest, but one should keep in mind that it would require between 100^2 to 600^2 times more scans to obtain a spectrum with the same SNR at thermal equilibrium, which would translate to 21 days to 2 years of uninterrupted acquisition considering an experimental repetition delay set to 3 min.

To our knowledge, these findings represent the first successful application of dDNP for the analysis of battery electrolytes. A high-sensitivity, well-resolved ^{13}C spectrum of an electrolyte solution at natural isotopic abundance was acquired in a single scan after dDNP using a custom-designed effective formulation protocol.

To demonstrate the practicability of this approach to more challenging samples, additional experiments were performed on electrolytes that were purposefully degraded. Two samples were investigated consisting of 1M of $LiPF_6$ salt in ethyl-methyl carbonate (EMC), with 3% wt vinylene carbonate (VC). The two electrolytes only differed by the presence (electrolyte A) or absence (electrolyte B) of an additive, tris(trimethylsilyl) phosphite (TMSPi), added in 5% wt. Both electrolytes were left to age on the shelf for a year at room temperature in aluminum containers. The goal here was to detect low-intensity signals corresponding to any degradation product, and assess any potential change due to the presence of the additive. For the dDNP experiments, the two samples were prepared following the protocol developed for the commercial electrolyte: 50 mM of TEMPO were directly added to the electrolyte solutions, and the latter were hyperpolarized at 7.05 T and 1.8 K. From the polarizing method to sample dissolution and spectrum acquisition in solution, the same workflow as presented earlier was implemented.

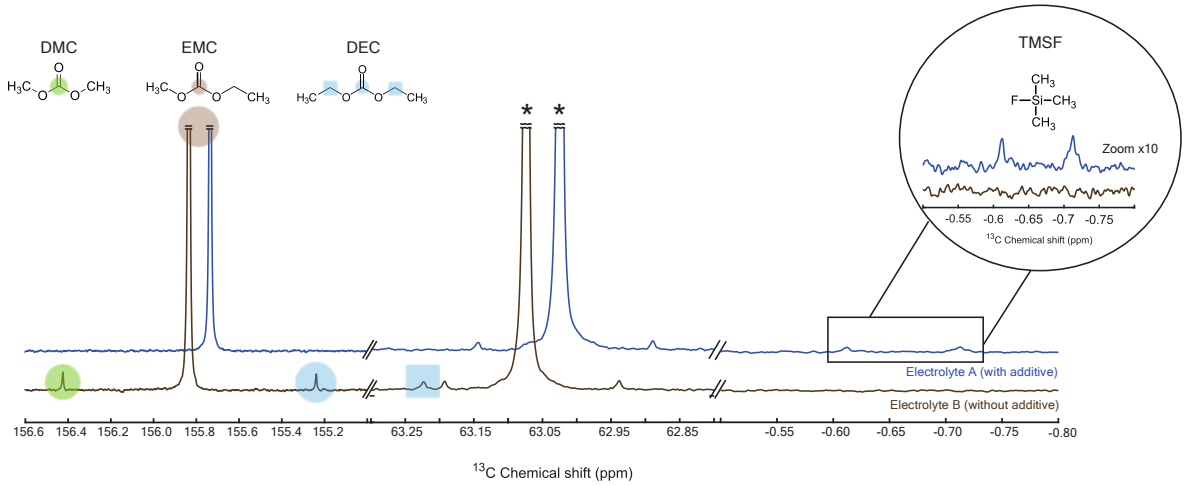

Figure 4: Hyperpolarized ^{13}C proton decoupled spectra of electrolyte A with additive (top, blue) and electrolyte B without additive (bottom, brown), highlighting regions of the spectra where differences could be found. Spectra were acquired right after dDNP with a single 90° hard pulse. Additional identified degradation peaks are highlighted with a green circle for dimethyl carbonate carbonyl group, a blue circle for diethyl carbonate carbonyl group, and a blue square for diethyl carbonate CH_2 groups. The presence of the degraded additive in the form of fluorotrimethylsilane (TMSF) was also detected on the electrolyte A spectrum as shown in the zoomed circular insert. The transesterification reaction responsible for the appearance of degradation peaks in electrolyte B is shown in Scheme 1. Signals marked with a star correspond to isopropanol signals.

Figure 4 shows the two hyperpolarized spectra obtained after dDNP on electrolyte A (blue) and electrolyte B (brown). Three additional peaks were identified in the electrolyte B spectrum at 156.4 ppm, 155.2 ppm, and 63.2 ppm. These signals could be attributed to transesterification products of the ethyl methyl carbonate, as shown in Scheme 1, based on the known chemical shifts for these two compounds and relevant literature[44,45]. This transesterification process occurs when the electrolyte

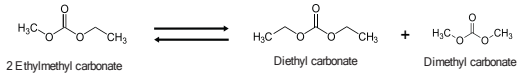

Scheme 1: Transesterification reaction of ethyl methyl carbonate into diethyl carbonate and dimethyl carbonate

degrades and is more pronounced at late degradation stages.

An additional doublet could also be identified in the spectrum of electrolyte A at a chemical shift of -0.66 ppm. This signal, which is absent on the electrolyte B spectrum, corresponds to TMSPi, and, more specifically, to its degradation compound, fluorotrimethylsilane (TMSF)[46,47]. Its signal was also found in the ^1H spectrum of the solution at 0.22 ppm (see SI Figure S4). TMSPi is known to act as both a water and HF scavenger and can also further react with degradation products produced by the reaction of $LiPF_6$ with water and HF[46].

The difference in degradation state between the two electrolytes could be attributed to the presence of the additive. The additive reacted with HF, preventing it from

being incorporated into the degradation pathway and thus slowing down the reaction. No other products could be identified in the ^{13}C spectra.

The polarization levels, and therefore enhancements, were much more modest than those achieved during the previous experiments with commercial electrolytes (see SI section 3, Table S3 and S4). The ^{1}H polarization build-up of the two electrolytes, compared to the commercial one (see SI figure S5), indicates that the DNP was less efficient than for fresh electrolyte solutions. This suggests that most of the radicals may not have survived in the highly degraded electrolyte. An EPR analysis of the solution was carried out (see SI section 4 and figure S6) and showed that the radicals were mostly quenched in degraded electrolytes. This can be explained by the formation of hydrofluoric acid (HF) in the solution resulting from $LiPF_6$ degradation[48,49]. The presence of HF can lead to the irreversible reduction of part, if not most, of the TEMPO radicals[50].

Although the enhancements are less than before, dDNP remains advantageous in terms of sensitivity compared to a thermal equilibrium experiment. The thermal equilibrium spectrum of electrolyte B was recorded after the dissolution experiments during 6 hours with 128 scans. The SNR/mM of each peak was calculated and compared to the value obtained with dDNP (see SI section 3, Table S5). These calculations show that given equal concentration, the SNR is, in the best case, 8 times better with dDNP. The same spectra under thermal equilibrium conditions would, therefore, require 16 days of uninterrupted acquisition.

These results show that even with suboptimal DNP conditions, dDNP remains advantageous, as it offers a non-negligible sensitivity boost translating into significant experimental timesaving. These results could potentially be improved by having more efficient DNP in the solid state, which would require using polarizing agents that can survive in degraded electrolytes. Recently, the use of epoxy-based polarizing agent (HYPOP), was introduced[51]. In these materials, the radicals are confined within the polymer's network. Using such polymers could be a solution to limit radical quenching in contact with the electrolyte and, therefore, greatly improve the polarization of the sample.

Access to the electrolyte's carbon content is particularly interesting as it is complementary to the information obtained with the analysis of other nuclei. It could, for instance, help to better characterize carbonate-derived species involved in SEI formation[52,53]. Carbon detection benefits from a wide spectral window and easy-to-implement sequences, which can allow for unambiguous identification and resolution of each carbon peaks, a key in the characterization of a molecule's structure. ^{1}H detection can also be useful to solve the analyte's puzzle. It is, in principle, more sensitive, but the spectrum is usually more difficult to assign and analyze due to the signals' multiplicity and the presence of large solvent signals. Detecting ^{1}H and ^{13}C hyperpolarized spectra in one dDNP experiment could be investigated in the future, as it was demonstrated recently for metabolomic studies[54]. Using the same approach for battery electrolytes could complement the results provided by ^{13}C spectra, and potentially give access to other degradation species that do not contain carbon atoms. Proton investigation with dDNP would also allow for sensitivity boosts that could push the ^{1}H detection limits to smaller traces, and further participate in deciphering what happens during the electrolyte's degradation.

Conclusion and outlooks

This work shows that dDNP can be applied to study battery electrolyte solutions using a simple sample formulation, only requiring the addition of polarizing agents to the electrolyte, without further modification of the sample. With this method, high sensitivity and well resolved ^{13}C spectra at natural abundance could be acquired with enhancements of two to three orders of magnitude, enabling the detection of all carbon species within each molecule of interest. This methodology allows for the detection of electrolyte solutions down to 30 µM, on natural abundance ^{13}C.

It is also demonstrated that the methodology can be used to investigate degraded electrolyte samples. Differences in the degradation stages of two electrolyte formulations, only differing by the presence or absence of a small amount of additive, could be highlighted in a single experiment instead of 16 days under conventional NMR conditions. The additive could also be detected at natural abundance, though it represented only 5% of the weight of the sample. These results show that the dDNP methodology can be adapted to study complex, hydrophobic samples such as battery electrolytes. However, performance on degraded electrolytes remains suboptimal due to the reduction of the radicals by the acidic degradation products. A further improvement for future studies would be to find a way to protect the radicals from reacting with the acidic environment of the electrolyte. An appealing alternative would be using hyperpolarizing matrices, such as HYPOP epoxy-resin-based materials in which TEMPO radicals are confined within the network of the polymer [55].

We believe this work will pave the way for future uses of dDNP in the field of battery investigation in a context where their development and optimization are particularly necessary and critical.

Material and Methods

Sample preparation

Commercial electrolyte sample

A solution of battery electrolyte made of 1M of $LiPF_6$ in ethylene carbonate (EC) and dimethyl carbonate (DMC) was purchased from Sigma Aldrich. 7.7 mg of TEMPO radicals purchased from Sigma Aldrich were then added to 1 mL of the electrolyte solution, the radical concentration was therefore 49.28 mM. 100 µL of the solution were then put in a PEEK custom sample holder. The sample holder was introduced shortly after in the polarizer at 3.8 K to instantly freeze the sample. The sample was briefly exposed to air and humidity during its preparation and insertion (less than 10 minutes). The sample preparation was done under a fume hood to make it as easy as possible. The brief sample exposure to air was not found to have an observable impact (see SI section 1)

Degraded electrolyte samples

Both degraded electrolytes were directly prepared and sent by SAFT. 500 µL of the electrolytes were withdrawn. For electrolyte A, 4.4 mg of TEMPO were added, leading to a radical concentration of 56.3 mM. For electrolyte B, 4.5 mg of TEMPO was added, leading to a radical concentration of 57.6 mM. The preparation of commercial battery electrolyte samples was done under a fume hood. 100 µL of the respective mixtures were added to a custom PEEK sample holder to be introduced in the polarizer.

DNP experiments

DNP experiments were realized on a 7.05 T Bruker dDNP Polarizer. The temperature of the cryostat in which the sample sits was cooled down with a Pfeiffer UNO 30M oil pump which allowed to reach temperatures down to 1.6 K.

A microwave source from Virginia Diodes Inc., Charlottesville, VA) operating in the range 196.8 - 198.8 GHz was used for microwave irradiations during DNP. DNP was performed by irradiating the sample with modulated microwave frequencies centered respectively around 197.57 GHz at 3.8 K and 197.65 GHz at 1.8 K. The output power used for these experiments was 100 mW at the output of the amplifier module, corresponding to a calculated 30 mW power reaching the sample's cavity. Modulation bandwidth was set in all cases at 128 MHz, and modulation frequency to 500 Hz.

All dDNP experiments on electrolytes were carried out in custom PEEK sample holders with 100 µL of sample. ^{1}H polarization build-up experiments and ^{13}C multi-CP experiments were performed on this type of sample cup at a temperature of approximately 1.8 K. ^{1}H polarization build-ups were monitored by recording the signal every 5 seconds with a 64 consecutive 0.1° pulses. Polarization was transferred from ^{1}H to ^{13}C using multi-CP experiments, with a sequence developed previously in the group that includes microwave gating. ^{13}C multi-CP experiments were realized at 1.8 K with the same microwave frequency, modulation parameters, and power. ^{13}C polarization build-up was followed by pulsing on the carbon every 2 min with a 5° detection pulse. A CP contact was made after waiting for an amount of time corresponding to the proton polarization build-up time at 1.8 K. For commercial electrolytes, this time corresponded to 8 min. 6 CP contacts were performed, leading to an experimental time of ~1h. For the degraded electrolytes, ^{13}C polarization build-up was followed by pulsing on the carbon every 3 min with a 5° detection pulse. A CP contact was made every 15 min, corresponding to the proton polarization build-up time at 1.8 K for these samples. 4 CP contacts were performed, leading to an experimental time of ~1h.

Integrals were calculated using TopSpin 3.6.4 software. The polarization build-up time, denoted τ_{DNP} was determined by plotting the Integral value as a function of time, following a stretched mono-exponential equation such as to account for the distribution of build-up times:

$$I = I_0 \times (1 - exp\,{}^{(\frac{-t}{\tau_{DNP}})^b})$$

I_0 corresponds to the initial intensity, τ_{DNP} corresponds to the build-up time, and b is the stretch coefficient characterizing the breadth of the build-up times distribution. Proton enhancements were determined by calculating the ratio between the integral of the DNP signal on the plateau of the build-up curve and the integral of a thermal equilibrium signal of the same sample. All integral values were normalized by their gain, number of scans, number of spins, temperature, pulse angle, and concentration, according to a protocol described elsewhere[32]. The final enhancement values were then corrected to account for the signal losses during the dead time of the spectrometer caused by radiation damping (RD)[56] (see section 5 in the SI).

Final proton polarizations were calculated by multiplying the corrected enhancement by the thermal equilibrium polarization of the ^{1}H at 7.05 T and 3.8 K.

Carbon enhancements were determined by calculating the ratio between the integral of the last ^{13}C signal of the multi-CP experiment before dissolution, at 1.8 K, and the integral of a ^{13}C thermal equilibrium signal of a reference 3M Acetate in dDNP juice sample (glycerol-d_8/D_2O/H_2O, 6/3/1, v/v/v + 50 mM TEMPO) at 3.8K. All integral values were normalized by their gain, number of scans, number of ^{13}C spins, temperature, pulse angle, and concentration in the same fashion as for proton calculations.

Final ^{13}C polarizations were determined by multiplying the enhancements with the thermal equilibrium ^{13}C polarization value at 7.05 T and 3.8 K

Dissolution

Dissolution experiments were carried as follows:

7 mL of dissolution solvent, a mix of isopropanol and deuterated isopropanol (3/1, v/v) was put in a heating chamber and pre-pressurized at 9 bars. The solvent was heated to 12 bars, corresponding to a temperature of 160°C while the multi-CP assisted DNP experiment was being performed. Once the polarization reached a plateau, the experiment was stopped (both CP and microwave irradiation), and the Polarizer cryostat was put under He pressure (1200 mbar) and opened to insert a dissolution stick. The dissolution stick was connected to the heating chamber through quick connects, and coupled manually with the sample cup. Dissolution was immediately triggered by pushing a button, releasing the hot pressurized solvent pushed with 9 bars inside the capillaries of the dissolution stick, thus melting and expelling the hyperpolarized sample to a fast injection system[37]. 600 µL of solution were selected by the fast injection system and propelled to the NMR tube in the acquisition spectrometer within 2 seconds. A magnetic tunnel composed of hand-coiled solenoids installed over the transfer capillaries ensured that the sample experienced a magnetic field of at least 5 mT, all the way to the NMR tube.

Liquid state NMR

Liquid state NMR experiments were realized at 14 T using a 5mm CP2.1 QCI 600S3 H-P/C/N-D-05 Z XT cryoprobe with gradients. The liquid was directly injected into a medium-thickness wall NMR tube attached to the dissolution transfer line, waiting inside the spectrometer. The ^{13}C hyperpolarized spectrum acquisition was started through a trigger at the end of the dissolution, transfer, and injection process. A resting time of 8 seconds was added before the beginning of the acquisition to let the solution

stabilize. Six 90° detection pulses were applied every 30 seconds with proton decoupling. The data were stored as a pseudo-2D experiment and the first 1D spectrum was extracted from these data sets.

Thermal equilibrium spectra after dissolution were acquired on the same dissolved sample, at 14 T, with the same cryoprobe after making sure hyperpolarization had completely decayed. The ^{13}C signal was recorded with proton decoupling in 8 scans using 90° hard pulses and a repetition time of 3 min. The total acquisition time was 24 min. ^{1}H thermal equilibrium spectrum was then acquired in one scan using a 90° hard pulse.

Enhancements were determined by calculating the ratio between the integral of the dDNP signal and the integral of a thermal equilibrium signal of known concentration. All integral values were normalized by their gain, number of scans, number of spins, and concentration. All experiments consisted of a $\pi/2$ hard pulse, so there was no need to normalize the pulse angle in this case.

Final polarizations were calculated by multiplying the enhancement with the thermal equilibrium polarization of the ^{13}C nucleus at 14 T and 298 K.

Final concentrations were determined with an external method: the signal integral of the ^{1}H spectrum recorded after dissolution was directly compared with the ^{1}H signal integral of the same compound in known concentration, recorded with the same experimental setup and parameters.

Acknowledgements

We acknowledge Bruker Biospin for providing the prototype dDNP polarizer and particularly D. Eshchenko, R. Melzi, M. Rossire, M. Sacher, and J. Kempf for scientific and technical support. We additionally acknowledge C. Jose and C. Pages for use of the ISA Prototype Service, and S. Martinez of the UCBL mechanical workshop for machining parts of the experimental apparatus. We also acknowledge SAFT for providing samples, more specifically E. Kherchiche and T. Sombret for preparing the samples, and A. Gajan for scientific support. We acknowledge C. Thieuleux from the CPE Lyon laboratory for providing access to their infrastructure for sample preparation. This research was supported by TotalEnergies, the French CNRS, the Université Claude Bernard de Lyon 1 (RUC633), and the National Association for Research and Technology (ANRT) (Convention CIFRE 2021/1509).

Authors contributions

CG, SL, SP and SJ conceived the experiment. CG and EP performed the experiments. CG analyzed the data. CG wrote the manuscript with SJ and SL. CB and JT provided technical support on the dDNP polarizer. AME provided technical assistance with the fast injection system. NL and LV provided technical assistance for sample preparation and glove box handling. SG, AL and SJ provided fundings and supervised the research. All authors contributed to refining the manuscript.

Data availability

The experimental data presented in this work, the MATLAB codes used to analyze them and the MATLAB codes used for all simulations can be downloaded from this link: **10.5281/zenodo.14041355**

Competing interests

The authors declare that they do not have any competing interests.

References

(1) Ardenkjær-Larsen, J. H.; Fridlund, B.; Gram, A.; Hansson, G.; Hansson, L.; Lerche, M. H.; Servin, R.; Thaning, M.; Golman, K. Increase in Signal-to-Noise Ratio of > 10,000 Times in Liquid-State NMR. *Proc. Natl. Acad. Sci. U.S.A.* **2003**, *100* (18), 10158–10163. https://doi.org/10.1073/pnas.1733835100.

(2) Wenckebach, W. T. *Essentials of Dynamic Nuclear Polarization*; Spindrift Publications, 2016.

(3) Comment, A. Dissolution DNP for in Vivo Preclinical Studies. *J Magn Reson* **2016**, *264*, 39–48. https://doi.org/10.1016/j.jmr.2015.12.027.

(4) Brindle, K. M. Imaging Metabolism with Hyperpolarized 13C-Labeled Cell Substrates. *J. Am. Chem. Soc.* **2015**, *137* (20), 6418–6427. https://doi.org/10.1021/jacs.5b03300.

(5) Rodrigues, T. B.; Serrao, E. M.; Kennedy, B. W. C.; Hu, D.-E.; Kettunen, M. I.; Brindle, K. M. Magnetic Resonance Imaging of Tumor Glycolysis Using Hyperpolarized 13C-Labeled Glucose. *Nat Med* **2014**, *20* (1), 93–97. https://doi.org/10.1038/nm.3416.

(6) Nelson, S. J.; Kurhanewicz, J.; Vigneron, D. B.; Larson, P. E. Z.; Harzstark, A. L.; Ferrone, M.; van Criekinge, M.; Chang, J. W.; Bok, R.; Park, I.; Reed, G.; Carvajal, L.; Small, E. J.; Munster, P.; Weinberg, V. K.; Ardenkjaer-Larsen, J. H.; Chen, A. P.; Hurd, R. E.; Odegardstuen, L.-I.; Robb, F. J.; Tropp, J.; Murray, J. A. Metabolic Imaging of Patients with Prostate Cancer Using Hyperpolarized [1- ^{13} C]Pyruvate. *Sci. Transl. Med.* **2013**, *5* (198), 1–22. https://doi.org/10.1126/scitranslmed.3006070.

(7) Dos Santos, K.; Bertho, G.; Caradeuc, C.; Baud, V.; Montagne, A.; Abergel, D.; Giraud, N.; Baudin, M. A Toolbox For Glutamine Use In Dissolution Dynamic Nuclear Polarization: From Enzymatic Reaction Monitoring To The Study Of Cellular Metabolic Pathways And Imaging. *ChemPhysChem* **2023**, e202300151. https://doi.org/10.1002/cphc.202300151.

(8) Salamanca-Cardona, L.; Keshari, K. R. 13C-Labeled Biochemical Probes for the Study of Cancer Metabolism with Dynamic Nuclear Polarization-Enhanced Magnetic Resonance Imaging. *Cancer Metab* **2015**, *3* (1), 1–11. https://doi.org/10.1186/s40170-015-0136-2.

(9) Ribay, V.; Dey, A.; Charrier, B.; Praud, C.; Mandral, J.; Dumez, J.-N.; Letertre, M. P. M.; Giraudeau, P. Hyperpolarized 13C NMR Spectroscopy of Urine Samples at Natural Abundance by Quantitative Dissolution Dynamic Nuclear Polarization. *Angew Chem Int Ed* **2023**, e202302110. https://doi.org/10.1002/anie.202302110.

(10) Dey, A.; Charrier, B.; Martineau, E.; Deborde, C.; Gandriau, E.; Moing, A.; Jacob, D.; Eshchenko, D.; Schnell, M.; Melzi, R.; Kurzbach, D.; Ceillier, M.; Chappuis, Q.; Cousin, S. F.; Kempf, J. G.; Jannin, S.; Dumez, J.-N.; Giraudeau, P. Hyperpolarized NMR

Metabolomics at Natural ^{13}C Abundance. *Anal. Chem.* **2020**, *92* (22), 14867–14871. https://doi.org/10.1021/acs.analchem.0c03510.

(11) Miclet, E.; Abergel, D.; Bornet, A.; Milani, J.; Jannin, S.; Bodenhausen, G. Toward Quantitative Measurements of Enzyme Kinetics by Dissolution Dynamic Nuclear Polarization. *J. Phys. Chem. Lett.* **2014**, *5* (19), 3290–3295. https://doi.org/10.1021/jz501411d.

(12) Hu, J.; Kim, J.; Hilty, C. Detection of Protein–Ligand Interactions by ^{19}F Nuclear Magnetic Resonance Using Hyperpolarized Water. *J. Phys. Chem. Lett.* **2022**, *13* (17), 3819–3823. https://doi.org/10.1021/acs.jpclett.2c00448.

(13) Cala, O.; Bocquelet, C.; Gioiosa, C.; Torres, F.; Cousin, S. F.; Guibert, S.; Ceillier, M.; Busse, V.; Decker, F.; Kempf, J. G.; Elliott, S. J.; Stern, Q.; Bornet, A.; Jannin, S. Micromolar Concentration Affinity Study on a Benchtop NMR Spectrometer with Secondary 13C Labeled Hyperpolarized Ligands. ChemRxiv April 24, 2024. https://doi.org/10.26434/chemrxiv-2024-s4t56.

(14) Jannin, S. Application and Methodology of Dissolution Dynamic Nuclear Polarization in Physical, Chemical and Biological Contexts. *Journal of Magnetic Resonance* **2019**.

(15) *Handbook of Batteries*, 3rd ed.; Linden, D., Reddy, T. B., Eds.; McGraw-Hill handbooks; McGraw-Hill: New York, 2002.

(16) Kanevskii, L. S.; Dubasova, V. S. Degradation of Lithium-Ion Batteries and How to Fight It: A Review. **2005**, *41* (1).

(17) Broussely, M.; Biensan, Ph.; Bonhomme, F.; Blanchard, Ph.; Herreyre, S.; Nechev, K.; Staniewicz, R. J. Main Aging Mechanisms in Li Ion Batteries. *Journal of Power Sources* **2005**, *146* (1), 90–96. https://doi.org/10.1016/j.jpowsour.2005.03.172.

(18) Schlasza, C.; Ostertag, P.; Chrenko, D.; Kriesten, R.; Bouquain, D. Review on the Aging Mechanisms in Li-Ion Batteries for Electric Vehicles Based on the FMEA Method. In *2014 IEEE Transportation Electrification Conference and Expo (ITEC)*; IEEE: Dearborn, MI, 2014; pp 1–6. https://doi.org/10.1109/ITEC.2014.6861811.

(19) Xu, K. Nonaqueous Liquid Electrolytes for Lithium-Based Rechargeable Batteries. *Chem. Rev.* **2004**, *104* (10), 4303–4418. https://doi.org/10.1021/cr030203g.

(20) Terborg, L.; Weber, S.; Blaske, F.; Passerini, S.; Winter, M.; Karst, U.; Nowak, S. Investigation of Thermal Aging and Hydrolysis Mechanisms in Commercial Lithium Ion Battery Electrolyte. *Journal of Power Sources* **2013**, *242*, 832–837. https://doi.org/10.1016/J.JPOWSOUR.2013.05.125.

(21) Markevich, E.; Salitra, G.; Aurbach, D. Fluoroethylene Carbonate as an Important Component for the Formation of an Effective Solid Electrolyte Interphase on Anodes and Cathodes for Advanced Li-Ion Batteries. *ACS Energy Lett.* **2017**, *2* (6), 1337–1345. https://doi.org/10.1021/acsenergylett.7b00163.

(22) Maddar, F. M.; Genieser, R.; Tan, C. C.; Loveridge, M. J. Monitoring Changes in Electrolyte Composition of Commercial Li-Ion Cells after Cycling Using NMR Spectroscopy and Differential Thermal Analysis. *J. Electrochem. Soc.* **2023**, *170* (3), 030522. https://doi.org/10.1149/1945-7111/acc365.

(23) Qian, Y.; Hu, S.; Zou, X.; Deng, Z.; Xu, Y.; Cao, Z.; Kang, Y.; Deng, Y.; Shi, Q.; Xu, K.; Deng, Y. How Electrolyte Additives Work in Li-Ion Batteries. *Energy Storage Materials* **2019**, *20*, 208–215. https://doi.org/10.1016/j.ensm.2018.11.015.

(24) Schmitz, R. W.; Murmann, P.; Schmitz, R.; Müller, R.; Krämer, L.; Kasnatscheew, J.; Isken, P.; Niehoff, P.; Nowak, S.; Röschenthaler, G.-V.; Ignatiev, N.; Sartori, P.; Passerini, S.; Kunze, M.; Lex-Balducci, A.; Schreiner, C.; Cekic-Laskovic, I.; Winter, M. Investigations on Novel Electrolytes, Solvents and SEI Additives for Use in Lithium-Ion Batteries: Systematic Electrochemical Characterization and Detailed Analysis by Spectroscopic Methods. *Progress in Solid State Chemistry* **2014**, *42* (4), 65–84. https://doi.org/10.1016/j.progsolidstchem.2014.04.003.

(25) Wiemers-Meyer, S.; Winter, M.; Nowak, S. NMR as a Powerful Tool to Study Lithium Ion Battery Electrolytes. In *Annual Reports on NMR Spectroscopy*; Elsevier, 2019; Vol. 97, pp 121–162. https://doi.org/10.1016/bs.arnmr.2018.12.003.

(26) Haber, S.; Leskes, M. Dynamic Nuclear Polarization in Battery Materials. *Solid State Nuclear Magnetic Resonance* **2022**, *117*, 101763. https://doi.org/10.1016/j.ssnmr.2021.101763.

(27) Yang, L.; Xiao, A.; Lucht, B. L. Investigation of Solvation in Lithium Ion Battery Electrolytes by NMR Spectroscopy. *Journal of Molecular Liquids* **2010**, *154* (2), 131–133. https://doi.org/10.1016/j.molliq.2010.04.025.

(28) Allen, J. P.; O'Keefe, C. A.; Grey, C. P. Quantifying Dissolved Transition Metals in Battery Electrolyte Solutions with NMR Paramagnetic Relaxation Enhancement. *J. Phys. Chem. C* **2023**. https://doi.org/10.1021/acs.jpcc.3c01396.

(29) Song, Z.; Zheng, L.; Cheng, P.; Wang, X.; Wu, H.; Ma, Q.; Liu, J.; Feng, W.; Nie, J.; Yu, H.; Huang, X.; Armand, M.; Zhang, H.; Zhou, Z. Taming the Chemical Instability of Lithium Hexafluorophosphate-Based Electrolyte with Lithium Fluorosulfonimide Salts. *Journal of Power Sources* **2022**, *526*, 231105. https://doi.org/10.1016/j.jpowsour.2022.231105.

(30) Golman, K.; Ardenkjaer-Larsen, J. H.; Petersson, J. S.; Månsson, S.; Leunbach, I. *Molecular Imaging with Endogenous Substances*; 2003. www.pnas.orgcgidoi10.1073pnas.1733836100.

(31) El Daraï, T.; Jannin, S. Sample Formulations for Dissolution Dynamic Nuclear Polarization. *Chem. Phys. Rev.* **2021**, *2* (4), 041308. https://doi.org/10.1063/5.0047899.

(32) Elliott, S. J.; Stern, Q.; Ceillier, M.; El Daraï, T.; Cousin, S. F.; Cala, O.; Jannin, S. Practical Dissolution Dynamic Nuclear Polarization. *Progress in Nuclear*

Magnetic Resonance Spectroscopy **2021**, *126–127*, 59–100. https://doi.org/10.1016/j.pnmrs.2021.04.002.

(33) Elliott, S. J.; Cala, O.; Stern, Q.; Cousin, S. F.; Ceillier, M.; Decker, V.; Jannin, S. Boosting Dissolution-Dynamic Nuclear Polarization by Multiple-Step Dipolar Order Mediated 1H→13C Cross-Polarization. *Journal of Magnetic Resonance Open* **2021**, *8–9* (100018), 1–6. https://doi.org/10.1016/j.jmro.2021.100018.

(34) Bornet, A.; Melzi, R.; Perez Linde, A. J.; Hautle, P.; van den Brandt, B.; Jannin, S.; Bodenhausen, G. Boosting Dissolution Dynamic Nuclear Polarization by Cross Polarization. *J. Phys. Chem. Lett.* **2013**, *4* (1), 111–114. https://doi.org/10.1021/jz301781t.

(35) Batel, M.; Krajewski, M.; Däpp, A.; Hunkeler, A.; Meier, B. H.; Kozerke, S.; Ernst, M. Dissolution Dynamic Nuclear Polarization Efficiency Enhanced by Hartmann–Hahn Cross Polarization. *Chemical Physics Letters* **2012**, *554*, 72–76. https://doi.org/10.1016/j.cplett.2012.10.018.

(36) Bornet, A.; Pinon, A.; Jhajharia, A.; Baudin, M.; Ji, X.; Emsley, L.; Bodenhausen, G.; Ardenkjaer-Larsen, J. H.; Jannin, S. Microwave-Gated Dynamic Nuclear Polarization. *Physical Chemistry Chemical Physics* **2016**, *18* (44). https://doi.org/10.1039/c6cp05587g.

(37) Ceillier, M.; Cala, O.; Daraï, T. E.; Cousin, S. F.; Stern, Q.; Guibert, S.; Elliott, S. J.; Bornet, A.; Vuichoud, B.; Milani, J.; Pages, C.; Eshchenko, D.; Kempf, J. G.; Jose, C.; Lambert, S. A.; Jannin, S. An Automated System for Fast Transfer and Injection of Hyperpolarized Solutions. *Journal of Magnetic Resonance Open* **2021**, *8–9*, 100017. https://doi.org/10.1016/J.JMRO.2021.100017.

(38) Bowen, S.; Hilty, C. Rapid Sample Injection for Hyperpolarized NMR Spectroscopy. *Phys. Chem. Chem. Phys.* **2010**, *12* (22), 5766–5770. https://doi.org/10.1039/C002316G.

(39) Milani, J.; Vuichoud, B.; Bornet, A.; Miéville, P.; Mottier, R.; Jannin, S.; Bodenhausen, G. A Magnetic Tunnel to Shelter Hyperpolarized Fluids. *Review of Scientific Instruments* **2015**, *86* (2). https://doi.org/10.1063/1.4908196.

(40) Lee, Y.; Heo, G. S.; Zeng, H.; Wooley, K. L.; Hilty, C. Detection of Living Anionic Species in Polymerization Reactions Using Hyperpolarized NMR. *Journal of the American Chemical Society* **2013**, *135* (12), 4636–4639. https://doi.org/10.1021/ja4001008.

(41) Harris, T.; Bretschneider, C.; Frydman, L. Dissolution DNP NMR with Solvent Mixtures: Substrate Concentration and Radical Extraction. *Journal of Magnetic Resonance* **2011**, *211* (1), 96–100. https://doi.org/10.1016/J.JMR.2011.04.001.

(42) Pender, J. P.; Jha, G.; Youn, D. H.; Ziegler, J. M.; Andoni, I.; Choi, E. J.; Heller, A.; Dunn, B. S.; Weiss, P. S.; Penner, R. M.; Mullins, C. B. Electrode Degradation in Lithium-Ion Batteries. *ACS Nano* **2020**, *14* (2), 1243–1295. https://doi.org/10.1021/acsnano.9b04365.

(43) Liao, Y.; Zhang, H.; Peng, Y.; Hu, Y.; Liang, J.; Gong, Z.; Wei, Y.; Yang, Y. Electrolyte Degradation During Aging Process of Lithium-Ion Batteries: Mechanisms, Characterization, and Quantitative Analysis. *Advanced Energy Materials n/a* (n/a), 2304295. https://doi.org/10.1002/aenm.202304295.

(44) Grützke, M.; Kraft, V.; Hoffmann, B.; Klamor, S.; Diekmann, J.; Kwade, A.; Winter, M.; Nowak, S. Aging Investigations of a Lithium-Ion Battery Electrolyte from a Field-Tested Hybrid Electric Vehicle. *Journal of Power Sources* **2015**, *273*, 83–88. https://doi.org/10.1016/j.jpowsour.2014.09.064.

(45) Campion, C. L.; Li, W.; Lucht, B. Thermal Decomposition of LiPF6-Based Electrolytes for Lithium-Ion Batteries. *Journal of The Electrochemical Society* **2005**, *152*, null. https://doi.org/10.1149/1.2083267.

(46) Qi, X.; Tao, L.; Hahn, H.; Schultz, C.; Gallus, D. R.; Cao, X.; Nowak, S.; Röser, S.; Li, J.; Cekic-Laskovic, I.; Rad, B. R.; Winter, M. Lifetime Limit of Tris(Trimethylsilyl) Phosphite as Electrolyte Additive for High Voltage Lithium Ion Batteries. *RSC Adv.* **2016**, *6* (44), 38342–38349. https://doi.org/10.1039/C6RA06555D.

(47) Jamal, A.; Salian, G. D.; Mathew, A.; Wahyudi, W.; Carvalho, R. P.; Gond, R.; Heiskanen, S. K.; Brandell, D.; Younesi, R. Tris(Trimethylsilyl) Phosphite and Lithium Difluoro(Oxalato)Borate as Electrolyte Additives for LiNi0.5Mn1.5O4-Graphite Lithium-Ion Batteries. *ChemElectroChem* **2023**, *10* (16), e202300139. https://doi.org/10.1002/celc.202300139.

(48) Wiemers-Meyer, S.; Winter, M.; Nowak, S. Mechanistic Insights into Lithium Ion Battery Electrolyte Degradation – a Quantitative NMR Study. *Phys. Chem. Chem. Phys.* **2016**, *18* (38), 26595–26601. https://doi.org/10.1039/C6CP05276B.

(49) Kawamura, T.; Okada, S.; Yamaki, J. Decomposition Reaction of LiPF6-Based Electrolytes for Lithium Ion Cells. *Journal of Power Sources* **2006**, *156* (2), 547–554. https://doi.org/10.1016/j.jpowsour.2005.05.084.

(50) Wylie, L.; Blesch, T.; Freeman, R.; Hatakeyama-Sato, K.; Oyaizu, K.; Yoshizawa-Fujita, M.; Izgorodina, E. I. Reversible Reduction of the TEMPO Radical: One Step Closer to an All-Organic Redox Flow Battery. *ACS Sustainable Chem. Eng.* **2020**, *8* (49), 17988–17996. https://doi.org/10.1021/acssuschemeng.0c05687.

(51) El Daraï, T.; Cousin, S. F.; Stern, Q.; Ceillier, M.; Kempf, J.; Eshchenko, D.; Melzi, R.; Schnell, M.; Gremillard, L.; Bornet, A.; Milani, J.; Vuichoud, B.; Cala, O.; Montarnal, D.; Jannin, S. Porous Functionalized Polymers Enable Generating and Transporting Hyperpolarized Mixtures of Metabolites. *Nat Commun* **2021**, *12* (4695), 1–9. https://doi.org/10.1038/s41467-021-24279-2.

(52) Yamaguchi, S.; Asahina, H.; Hirasawa, K. A.; Sato, T.; Mori, S. SEI Film Formation On Graphite Anode Surfaces In Lithium Ion Battery. *Molecular Crystals and Liquid Crystals Science and Technology. Section A. Molecular Crystals and Liquid Crystals* **1998**, *322* (1), 239–244. https://doi.org/10.1080/10587259808030230.

(53) Peled, E.; Golodnitsky, D.; Ardel, G. Advanced Model for Solid Electrolyte Interphase [SEI] Electrodes in

Liquid and Polymer Electrolytes. *Journal of The Electrochemical Society - J ELECTROCHEM SOC* **1997**, *144*. https://doi.org/10.1149/1.1837858.

(54) Dey, A.; Charrier, B.; Ribay, V.; Dumez, J.-N.; Giraudeau, P. Hyperpolarized 1H and 13C NMR Spectroscopy in a Single Experiment for Metabolomics. *Anal. Chem.* **2023**. https://doi.org/10.1021/acs.analchem.3c02614.

(55) Daraï, T. E.; Cousin, S. F.; Stern, Q.; Ceillier, M.; Kempf, J.; Eshchenko, D.; Melzi, R.; Schnell, M.; Gremillard, L.; Bornet, A.; Milani, J.; Vuichoud, B.; Cala, O.; Montarnal, D.; Jannin, S. Porous Functionalized Polymers Enable Generating and Transporting Hyperpolarized Mixtures of Metabolites. *Nature Communications* **2021**, *12* (1). https://doi.org/10.1038/s41467-021-24279-2.

(56) Stern, Q. Polarization Transfers in Dissolution Dynamic Nuclear Polarization from the Solid-State at High-Field to the Liquid-State at Zero-Field. phdthesis, Université Claude Bernard - Lyon I, 2022. https://theses.hal.science/tel-04238663 (accessed 2024-09-09).